

Nonlinear control solutions to prevent slugging flow in offshore oil production

Esmaeil Jahanshahi, Sigurd Skogestad

Department of Chemical Engineering, Norwegian University of Science and Technology (NTNU), NO-7491 Trondheim (e-mail: skoge@ntnu.no)

Abstract

Feedback control is an efficient and economical solution to prevent slugging flow regimes in offshore oil production. For this, a choke valve at the topside platform is used as the manipulated variable to control the pressure or the flow rate in the pipeline. The primary challenge for anti-slug controllers is robustness. The lack of robustness is due to changes in inflow conditions, the process nonlinearity, and modeling errors. In particular, the nonlinearity combined with an inverse response behavior makes the control of the topside pressure more difficult. We have conducted nonlinear and linear analysis and evaluated four control designs experimentally with both subsea and topside pressures. The control designs are 1) feedback linearization with measured outputs, 2) gain-scheduling IMC (internal model control) based on identified model, 3) PI control with an adaptive gain based on a static gain model, and 4) state feedback with state estimation by a nonlinear high-gain observer. We compared the robustness of these controllers regarding tolerance to time delay, change of the operating point and inflow disturbances. All the controllers could handle 30% step changes (disturbances) in inflow rates and remained stable. The gain-scheduling controller was more robust against time delay than the other controllers. By applying the high-gain observer, the stabilization was achieved in an acceptable range when only the topside pressure was available. However, the observer diverges when using a subsea pressure measurement which from a controllability point of view should be the easiest controlled variable. Nevertheless, this result agrees with the observability theory.

Keywords: Oil production, anti-slug control, unstable system, non-minimum-phase system, robust control

1. Introduction

In offshore oil production, a multi-phase mixture of oil, gas and water is transported from the producing oil wells at the seabed to the topside facilities through subsea pipelines and risers. Under certain inflow conditions (*i.e.* low inflow rates and low pressure), slugging flow regimes occur in the pipeline-riser systems. Such flow regimes are characterized by severe flow and pressure oscillations. These flow conditions cause numerous operational problems in oil production, *e.g.*, poor separation, overflow of inlet separators and unwanted gas flaring [1].

The conventional solution to mitigate slugging flow is to reduce the opening of the topside choke valve (choking), but this increases the back-pressure on the producing oil wells and decreases the production rate. Therefore, a solution that guarantees stable flow together with the maximum possible production rate is desirable.

Feedback control has been shown to be an effective strategy to eliminate slugging [2, 3, 4]. The topside choke valve is usually used as the control input to regulate pressure at a given pressure setpoint. Such a system is referred to as “anti-slug control” aiming to stabilize the flow under operating conditions that, without control, would lead to slugging [5]. Usually, a subsea pressure measurement is used as the controlled variable. The subsea pressure sen-

sor can be installed at the riser base (P_{rb}) or upstream towards the pipeline inlet (P_{in}). Controlling the pressure measured from the riser top (P_{rt}) is an alternative which is simpler from a practical point of view.

Although the control structures used for this purpose are simple, the existing anti-slug controllers are not robust in practice over long periods of operation. The robustness issues are mainly due to varying inflow conditions, *i.e.* pressure, inflow rate and GOR (gas/oil ratio). “The slugging potential and flow regime change over time. For example, the production engineers may add a new well to the manifold at the pipeline inlet, or they may close or open an incoming well stream for the production optimization reason. By adding a well, the total inflow rate may increase such that there will be no need for the slug control anymore. Then, one year later, the GOR may change, or the flow rate may increase or decrease. As a result, the system will experience a very different type of slugging. Therefore, it is not possible to develop a slug controller that can be left alone to handle all kinds of flow regimes, unfortunately. Changes in the operating conditions will require tight follow-up from someone who understands both multiphase flow and feedback control to update the controller settings. Such issues are not explained in the public domain literature. Most papers either present simulations or success stories” [6].

The nonlinearity of the process is a problem for a linear controller because the process gain changes drastically at different operating conditions, and the controller needs to be re-tuned. The nonlinearity of the process can be counteracted by nonlinear model-based controllers or by a gain-scheduling of linear controllers. Also, the effective time delay caused by long flowlines is another problematic factor for stabilizing control.

The primary objective of our research is to design robust anti-slug control systems. A robust controller requires less frequent re-tuning. The focus of this article is on nonlinear control solutions to counteract the process nonlinearity. First, we design a feedback linearization controller based on a mechanistic model. This controller uses two measured outputs (P_{rb} and P_{rt}). Another approach, in which the mechanistic model is not directly used for the control design, is to identify an unstable model of the system by a closed-loop step test. We use the identified model for an IMC (internal model control) design to control the inlet pressure (P_{in}). We construct gain-scheduling using three IMC controllers to cover a wide operational range. Next, we consider adaptive PI control where the adaptation is based on a simple model for the static nonlinearity of the process. Here, the controlled variable of the feedback is the inlet pressure (P_{in}), and the static process gain is updated from the valve opening value (Z) and the topside pressure (P_{rt}) which are always available.

Stabilizing control using only the topside pressure measurement (P_{rt}) is not robust; this has been investigated based on a linear controllability analysis [7]. If only the topside pressure measurement is available, a conventional control solution is to design an observer to estimate the states of the system including the subsea pressure, and then use these estimates for control [8, 9]. Although we know that the observer and the state feedback design cannot be generalized for all control application, we will investigate if this solution can recover some stabilizability and robustness when no subsea measurement is available.

Some of the results provided in the paper have been partially presented in [10]. In this article, we add a system analysis and the adaptive control design, and we discuss the results in detail.

This article is organized as follows. A mechanistic model for the severe slugging flow is introduced in Section 2, and the model is used for analysis in Section 3. The four control designs are presented in Section 4. The experimental results are shown in Section 5 and discussed in Section 6. Finally, the main remarks and conclusions are summarized in Section 7.

2. First Principle Model

We have developed a dynamic model for riser slugging based on mass and momentum balances [5]. This model is able to capture the main dynamics of the slugging flow regime, and it is of good fit with the detailed commercial simulator OLGA[®] [11] and experiments. The model is

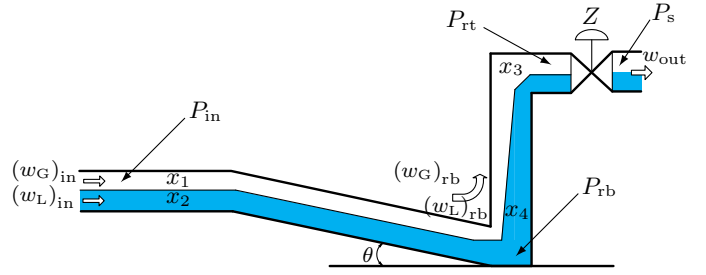


Figure 1: Schematic presentation of the system

described by only four ODEs with soft nonlinear functions which make it suitable for controller design.

2.1. Summary of the four-state model

Figure 1 shows a schematic presentation of the model. The state variables of this model are

- x_1 [kg]: mass of gas in pipeline
- x_2 [kg]: mass of liquid in pipeline
- x_3 [kg]: mass of gas in riser
- x_4 [kg]: mass of liquid in riser

The four state equations of the model are the following mass balances:

$$\dot{x}_1 = (w_G)_{in} - (w_G)_{rb} \quad (1)$$

$$\dot{x}_2 = (w_L)_{in} - (w_L)_{rb} \quad (2)$$

$$\dot{x}_3 = (w_G)_{rb} - (\alpha_G^m)_{rt} w_{out} \quad (3)$$

$$\dot{x}_4 = (w_L)_{rb} - [1 - (\alpha_G^m)_{rt}] w_{out} \quad (4)$$

The inflow rates of gas and liquid to the system, $(w_G)_{in}$ and $(w_L)_{in}$, are assumed to be independent disturbances with known nominal values. The flow rates of gas and liquid from the pipeline to the riser, $(w_G)_{rb}$ and $(w_L)_{rb}$, are described by virtual valve equations (A.30), (A.33). The outlet mixture flow rate, w_{out} , is determined by the opening percentage of the topside choke valve, Z , which is the manipulated variable of the control.

Although (1)-(4) seem to be linear, calculation of the flow rates and the mass fraction $(\alpha_G^m)_{rt}$ involves several nonlinear equations (*e.g.* valve equations and frictions). See Appendix A for the complete set of the model equations.

2.2. Model fitting

The four-state model can be partly configured based on dimensions and other physical properties (*e.g.* fluid properties) to fit it to a given pipeline-rise system. In addition, four fitting parameters are included in the model for the purpose of fine-tuning. The fitting procedure is described in [5]. In this work, the four-state model has

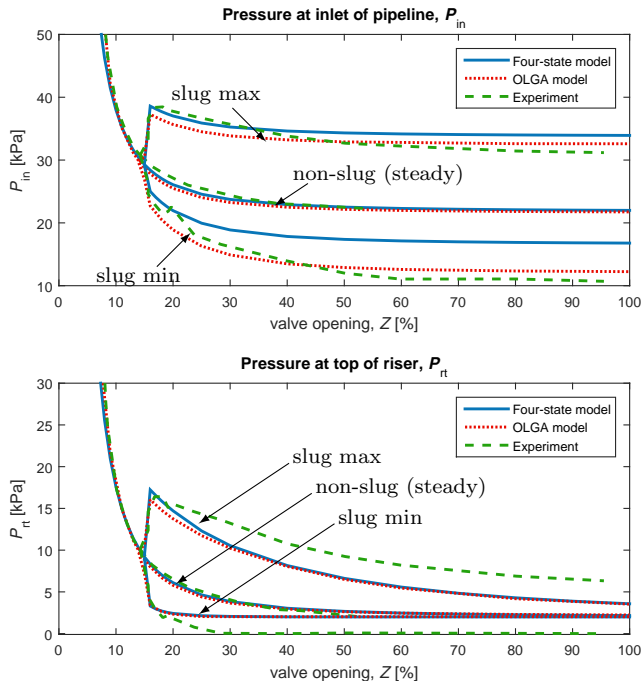


Figure 2: Bifurcation diagrams of four-state model (blue) compared to OLGA model (red) and experiments (green)

been fitted to data from experiments and simulations using the OLGA simulator. The experimental setup is described in Section 5.1.

The open-loop system has a stable (non-slugging) flow when Z is smaller than 15%, and it switches to unstable (slugging) flow conditions for larger valve openings. The bifurcation diagram describes steady-state process values and the minimum and maximum values when the flow is oscillatory [7]. This diagram may be obtained experimentally or from a more detailed model (*e.g.* OLGA). Such diagrams are used as the reference to fit the model (Figure 2).

In Figure 2, the minimum and maximum values for the four-state model deviate from those of OLGA and the experiment. These differences are due to measurement noises and un-modeled dynamics such as hydrodynamic slugging, which the four-state model is not able to describe. From a control point of view, the steady flow (middle line) is more important, because it represents equilibrium points where the controlled system operates on.

3. System Analysis

The desired steady-state (middle line) at the slugging condition ($Z > 15\%$) is unstable, but it can be stabilized by using control. The slope of the steady-state line is the static gain of the system, $G = \partial y / \partial u = \partial P_{in} / \partial Z$. As the valve opening increases this slope decreases, and the gain finally approaches zero. The small process gain makes control of the system with large valve openings difficult.

3.1. Nonlinearity analysis of the model

Here, we evaluate and compare the nonlinearity of the process seen from the different outputs and states by a nonlinearity measure. The present process is open-loop unstable in the desired region, and a closed-loop nonlinearity measure is required. We apply the optimal closed-loop nonlinearity measure proposed in [12],

$$\phi_{NOCL} := \inf_{L \in \mathcal{G}} \sup_{\mathbf{x}_0 \in \beta} \frac{\|N_{OCL}[\mathbf{x}_{x_0}^*] - L[\mathbf{x}_{x_0}^*]\|_{L_2}}{\|N_{OCL}[\mathbf{x}_{x_0}^*]\|_{L_2}} \quad (5)$$

with $N_{OCL}[\mathbf{x}_{x_0}^*] := \mathbf{u}_{x_0}^*$ and $\mathbf{x}_{x_0}^*$ being the solution to the infinite horizon control problem for the initial condition x_0 . In (5), $L[\mathbf{x}_{x_0}^*]$ represents the output of the optimal controller applied to the best linear approximation of the nonlinear process. The nonlinearity measure ϕ_{NOCL} must be close to 0 for a linear system.

For this analysis, we have made the inflow rates pressure-driven which is closer to the reality. For this, we have applied a linear IPR (Inflow Performance Relationship) as follows.

$$w_{in} = C_{PI} \max(P_{sour} - P_{in}, 0), \quad (6)$$

where C_{PI} is the Productivity Index and P_{sour} is the source pressure. To implement the nonlinearity measure, we stabilized the process by a \mathcal{H}_∞ optimal controller [13], then introduced setpoint changes in two directions (\pm) to move the process from the initial state x_0 . The setpoint change in the negative direction (towards a lower process gain) was obviously more difficult, and more simulations with the negative setpoint became unstable. The results for $Z = 30\%$ are summarized in Table 1.

All the controlled variables (CVs) are scaled so that setpoint changes to different CVs make the same change in the pressure. For the small setpoint changes (0.1 kPa), the system remained in the linear region, and the nonlinearity measure was close to 0. However, for a 1 kPa change, the nonlinearity measure became around $\phi_{NOCL} = 0.4$ when the valve opening (Z) is the manipulated variable. It is not possible to control P_{rt} , x_2 and x_3 by manipulating the valve opening for the large setpoint changes. We will discuss the reason later in this paper.

Next, we considered the outlet flow rate as a virtual control input, denoted by w' . Surprisingly, the nonlinearity measure is close to 0 even for large setpoint changes.

The nonlinearities seen from the valve input to all CVs are approximately the same, and $\phi_{NOCL} = 0.4$ is quite high for only a 1 kPa setpoint change. On the contrary, the process remains approximately linear for all outputs when the flow rate w' is the input. This analysis suggests that the nonlinearity is mostly caused by the valve equation relating the valve opening to the flow,

$$w_{out} = C_v f(Z) \sqrt{\rho_{rt} \Delta P_v}, \quad (7)$$

although a linear valve (*i.e.* $f(Z) = Z$) has been considered in the simulations. In (7), ΔP_v is the pressure drop over the valve, and ρ_{rt} is the mixture density.

Table 1: Nonlinearity analysis results (larger number indicates higher nonlinearity, and † denotes unstable response).

input	Δr	output						
		P_{in}	P_{rt}	w_{out}	x_1	x_2	x_3	x_4
Z	± 0.1	0.039	0.037	0.040	0.039	0.037	0.034	0.038
	± 1	0.414	†	0.431	0.414	†	†	0.404
w'	± 0.1	0.000	0.000	-	0.000	0.000	0.000	0.000
	± 1	0.003	0.003	-	0.001	0.006	0.006	0.005

3.2. Linear analysis

The steady-state behaviors of P_{in} and P_{rt} in Figure 2 are very similar; the difference is only a constant offset. However, the control system using P_{rt} becomes unstable with large setpoint changes (Table 1). Obviously, only the gain magnitude cannot describe all issues related to control of a dynamic system. Here, we analyze the dynamics in the frequency domain. Figure 3 shows the response of the topside pressure to a step change in the valve opening from 13% to 14%. The response of the four-state model is compared to the OLGA model which shows the relevance of the four-state model for our analysis. The inverse response behavior in the time domain translates to RHP zeros in the frequency domain. Figure 4 shows the Bode plot of the transfer function from the valve to P_{rt} . The phase is inverted at high frequencies. That is, the gain of the system is multiplied by -1 at high frequencies. This happens for the valve openings 20-40% where RHP poles exist, and their location is close to the RHP zeros. For $Z = 30\%$, the transfer function of the topside pressure P_{rt} has two unstable poles at $0.0816 \pm 0.1250i$ and two RHP-zeros at 0.13 and 0.4199.

The inlet pressure P_{in} does not have any RHP-zero in the desired region 20-40%. The same analysis has been undertaken for the four state variables too. The first state x_1 behaves similarly to the inlet pressure. The second and third states x_2 and x_3 show RHP-zero dynamics similar to P_{rt} , and both states have small gains. Hence, it is difficult to control them.

It is worth to point out that the process is open-loop stable from the input w' . As a result, from this input to all outputs, the RHP zeros dynamics are not limiting the controllability too much.

4. Control Designs

4.1. Feedback-linearizing controller

The two measurements used by the controller are the riser base pressure $y_1 = P_{rb}$ (riser base pressure) and the topside pressure $y_2 = P_{rt}$ (riser top pressure). We define the smooth function

$$F(y) := c \left(1 - \frac{y_2}{a} \right) \frac{a\alpha + y_2(1 - \alpha)}{bc - (y_1 - y_2 - F_r)}, \quad (8)$$

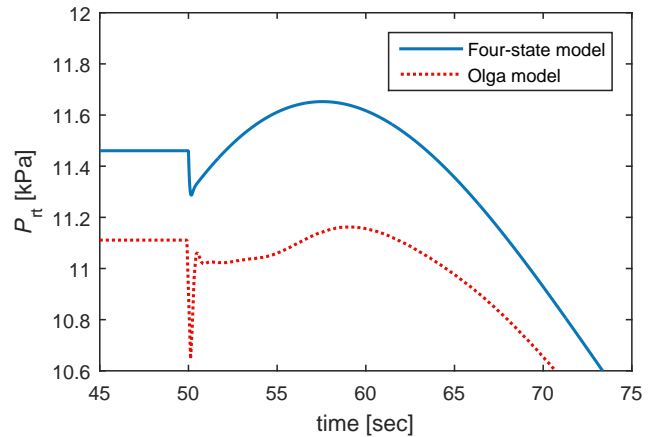


Figure 3: Open-loop response of topside pressure to a step change in the valve opening from 13% to 14%

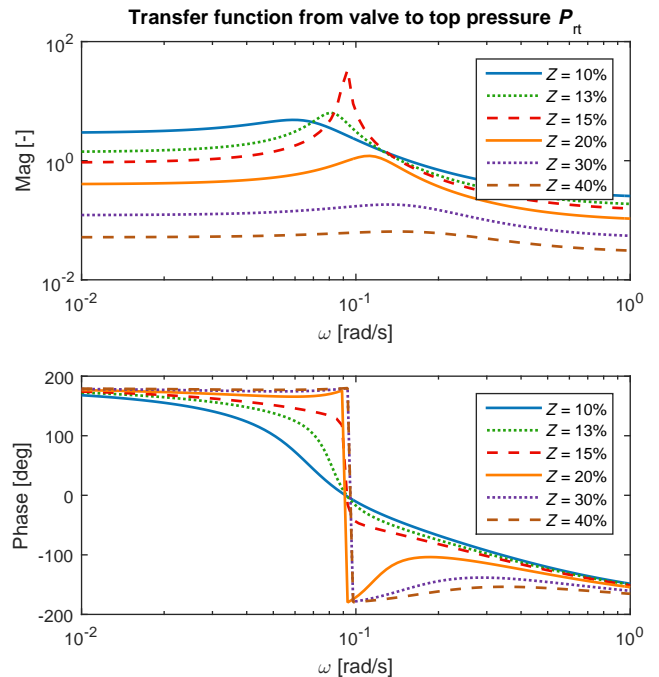


Figure 4: Bode plot of transfer function for topside pressure

where $a = RT_r \rho_l / M_G$, $b = \rho_l V_r$ and $c = g L_r / V_r$ are constant parameters. F_r is the friction in the riser which is assumed to be constant, and α is the average gas mass fraction. The virtual control input is

$$w' = \frac{w_{\text{in}}(F(y) + c) + K_1(y_1 - \bar{y}_1)}{F(y) + c}, \quad (9)$$

where $K_1 > 0$ and $w_{\text{in}} = (w_G)_{\text{in}} + (w_L)_{\text{in}}$ is the constant inlet flow rate to the system. \bar{y}_1 is the steady-state value or the setpoint. The final control signal to the valve is

$$u = \text{sat} \left(\frac{w'}{C_v \sqrt{\rho_{\text{rt}}(y_2 - P_s)}} \right), \quad (10)$$

where C_v and P_s are the choke valve constant and the separator pressure, respectively. The riser friction function F_r and the density ρ_{rt} are calculated based on the two pressure measurements y_1 and y_2 and model parameters. Derivation details of the control law and a proof for the closed-loop stability are described in [14].

It is a well-known fact that flow control removes the nonlinearity of valves. In the system analysis, we showed that the process is fairly linear if the outlet flow rate w' is the control input. In practice, a cascade controller is used where flow control is the inner loop, and the outer loop controls a pressure. However, this requires flow measurement that is often challenging and expensive for the multiphase flow. The control law described by (9) and (10) is a virtual flow controller where the flow is estimated by the model.

4.1.1. Controllability limitations

When using $y_1 = P_{\text{rb}}$ for feedback linearization in (9), the controller counteracts the nonlinearity, and it stabilizes the process in a wide range of valve opening values. However, this requires a large controller gain for large valve openings. We face two fundamental limitations when controlling P_{in} or P_{rb} with large valve openings:

Input saturation: The required control action is expressed as follows.

$$u = KS(r - G_d d - n)$$

Using an integral action, we reach the steady-state where the complementary sensitivity transfer function is $T \approx 1$. That is $KS = G^{-1}T \approx G^{-1}$. Thus, small G translates to a large KS and leads to large inputs due to measurement noises or disturbances. In other words, the controller cannot differentiate between noises and the unstable dynamics; it amplifies the noises, and the control signal becomes very aggressive.

Time delay: Time delay causes problems especially when controlling with a large valve opening because the unstable poles moves further away from the origin ("faster instability"). In addition, by increasing the controller gain (K) the delay margin of the control loop (θ_M) decreases, because the crossover frequency ω_c increases for a large controller gain (fast control action) and $\theta_M = (\text{PM})/\omega_c$.

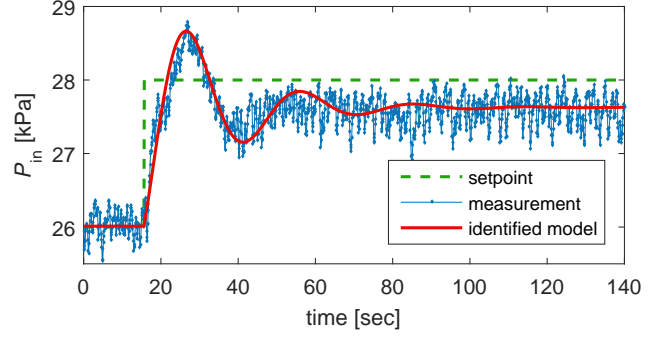


Figure 5: Response to step change in setpoint, obtained from experiments where process is stabilized by a proportional controller $K_{c0} = -10$. This response is only used for model identification.

4.2. Gain-scheduling IMC

It is possible to identify a linear unstable model of the system from a closed-loop step test (see Figure 5) as described by [15]. Here, P_{in} is the output, and the identified model contains two unstable poles and one stable.

$$G(s) = \frac{\hat{b}_1 s + \hat{b}_0}{s^2 - \hat{a}_1 s + \hat{a}_0} = \frac{k'(s + \varphi)}{(s - \pi_1)(s - \pi_2)} \quad (11)$$

We used the identified model for an IMC design [16]. The feedback version of the IMC controller becomes

$$C(s) = \frac{[\frac{1}{k'\lambda^3}](\alpha_2 s^2 + \alpha_1 s + 1)}{s(s + \varphi)}, \quad (12)$$

where λ is an adjustable filter time constant. The filter coefficients α_1 and α_2 are calculated by solving the following system of linear equations:

$$\begin{pmatrix} \pi_1^2 & \pi_1 & 1 \\ \pi_2^2 & \pi_2 & 1 \end{pmatrix} \begin{pmatrix} \alpha_2 \\ \alpha_1 \\ \alpha_0 \end{pmatrix} = \begin{pmatrix} (\lambda\pi_1 + 1)^3 \\ (\lambda\pi_2 + 1)^3 \end{pmatrix} \quad (13)$$

We chose $\alpha_0 = 1$ to achieve integral action in the controller. The closed-loop model identification and the IMC design for the slugging flow system are presented in [15] in greater detail.

For a gain-scheduling design, we identified three linear models from step tests at three different operating points, $P_{\text{in}} = 26$ kPa, $P_{\text{in}} = 23$ kPa and $P_{\text{in}} = 21.5$ kPa. Then, we designed three IMC controllers based on these identified models. The identified models and the resulting IMC controllers are given in Table 2. Switching (gain-scheduling) between the three controllers is based on the pressure setpoint and bump-less transfers between the controllers are implemented.

Note that we have used the setpoint (y_s) rather than the actual pressure (y) for the gain-scheduling logic because the setpoint (y_s) represents the steady-state that the system operates on and, in the case of a setpoint change, it determines the steady-state we want to approach. Besides, a given setpoint is a deterministic signal that is not

affected by noise. Thus, the gain-scheduling by setpoint does not suffer from random switching between controllers.

4.3. Adaptive PI Control

We consider a PI controller and adapt the proportional gain at different operating points to counteract the non-linearity of the system. This can be implemented as a gain-scheduling or an adaptive controller. The gain-scheduling or adaptation is based on the static gain of the system.

The middle line in the bifurcations diagrams (Figure 2) represents the desired non-slug flow. The slope of this line ($\frac{\partial y}{\partial u} = \frac{\partial P}{\partial Z}$) represents the process gain. We found that this curve follows the valve equation (7). Similarly, it was deduced from the nonlinearity analysis that the static nonlinearity is mainly caused by the valve equation.

The details of the static gain model are presented in Appendix B where the final model is given by (B.14). Assuming a linear valve (*i.e.* $f(Z) = Z$), the model is given as follow.

$$G_0 = \Delta G \left(\frac{-2(\Delta P_v)_{ss}}{Z_{ss}} \right), \quad (14)$$

where ΔG depends on the inflow rates and the density:

$$\Delta G = \frac{\rho_G^2 + c_1 \Delta P_r \alpha_G^m}{\rho_G^2 + c_1 \Delta P_v \alpha_G^m}, \quad (15)$$

where $c_1 = M_G/(RT_r)$, $\Delta P_r = \rho_{ss} g L_r$ and α_G^m is the gas mass fraction calculated from the inflow rates, $\alpha_G^m = (w_G)_{in} / [(w_G)_{in} + (w_L)_{in}]$. The steady state density ρ_{ss} is obtained from (B.4).

For the present case study, $0.9 < \Delta G < 1.1$ on the operation range of the valve, $5 \leq Z \leq 100$. Therefore, we can apply the following approximation:

$$G_0 \cong \frac{-2(\Delta P_v)_{ss}}{Z_{ss}} \quad (16)$$

Next, we formulate the adaptive controller as follows.

$$u = K_{ad} u_{bl}, \quad (17)$$

where u_{bl} denotes the baseline control signal and K_{ad} is an adaptive gain that is equal to 1 when controller operates in the baseline mode. We consider a PI controller as the baseline controller:

$$K_{bl}(s) = K_c \left(1 + \frac{1}{\tau_I s} \right) \quad (18)$$

The baseline PI tuning is obtained by considering the high- and low-frequency asymptotes of $C(s)$ in (12).

$$K_c = \lim_{s \rightarrow \infty} C(s) = \frac{\alpha_2}{k' \lambda^3} \quad (19)$$

$$\tau_I = \frac{K_c}{\lim_{s \rightarrow 0} sC(s)} = \alpha_2 \varphi \quad (20)$$

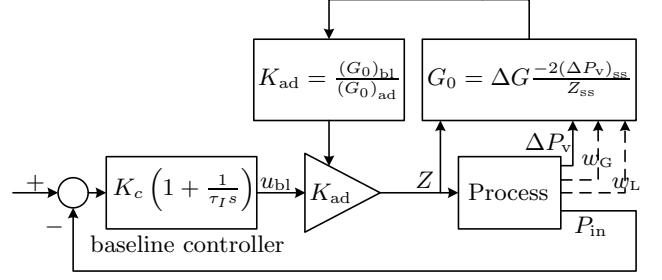


Figure 6: Structure of adaptive PI control where adaptation is based on ΔP_v and Z . A more accurate model can be applied if flow rates are available.

The adaptive gain is calculated based on the static gain model.

$$K_{ad} = \frac{(G_0)_{bl}}{(G_0)_{ad}}, \quad (21)$$

where $(G_0)_{bl}$ is the static gain at the design point of the baseline PI controller. That is the operating point where the closed-loop step test was preformed.

A block diagram for the adaptive control structure is shown in Figure 6. The input Z , the output ΔP_v and the inflow rates (if available) are used to calculate $(G_0)_{ad}$ from (14) or (16). Identical low-pass filters are applied on these measurements before calculating the static gain. The filtering reduces the noise effect on the controller performance, and it allows us to adjust the adaptation speed by tuning the time constant of the filters.

4.4. State feedback with nonlinear observer

The state variables x which are the masses of gas and liquid phases in the pipeline and the riser are not measurable, hence, we need to use their estimates \hat{x} in a state-feedback controller (Figure 7).

For linear systems, the *separation principle* allows us to separate the design into two tasks. First, we design a state feedback controller that stabilizes the system and meets other design specifications. Then an output feedback controller is obtained by replacing the state x by its estimate \hat{x} provided by observers. However, the *separation principle* does not hold in general for nonlinear systems, and we have to test this solution for the anti-slug control by experiments. For this, we designed a Luenberger-type nonlinear high-gain observer [17].

4.4.1. Control law

As shown in Figure 7, we apply full state feedback by using the estimated states. In addition, to prevent drift from the operating point, integral action is added by integrating the setpoint deviation for the estimated inlet pressure (\hat{P}_{in}). The total control action can be expressed as

$$u(t) = -K_c(\hat{x}(t) - x_{ss}) + K_i \int_0^t (\hat{P}_{in}(\tau) - r) d\tau. \quad (22)$$

Table 2: Gain-scheduling design

design point	identified model	IMC controller	gain-scheduling logic
$P_{\text{in}} = 26 \text{ kPa}$	$G_1(s) = \frac{-0.015(s+0.26)}{s^2-0.045s+0.0094}$	$C_1(s) = \frac{-16.15(s^2+0.016s+0.0012)}{s(s+0.26)}$	$P_{\text{set}} \geq 24 \text{ kPa}$
$P_{\text{in}} = 23 \text{ kPa}$	$G_2(s) = \frac{-0.0098(s+0.25)}{s^2-0.040s+0.025}$	$C_2(s) = \frac{-42.20(s^2+0.052s+0.0047)}{s(s+0.25)}$	$24 \text{ kPa} > P_{\text{set}} > 21.5 \text{ kPa}$
$P_{\text{in}} = 21.5 \text{ kPa}$	$G_3(s) = \frac{-0.0056(s+0.27)}{s^2-0.017s+0.096}$	$C_3(s) = \frac{-115.11(s^2+0.052s+0.014)}{s(s+0.27)}$	$P_{\text{set}} \leq 21.5 \text{ kPa}$

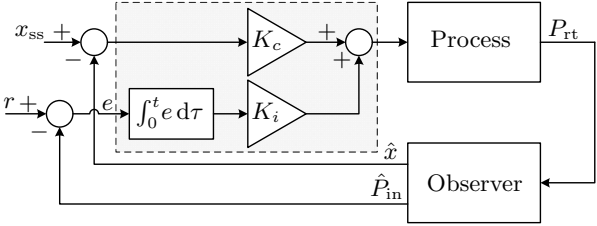


Figure 7: Block diagram of closed-loop system with observer and state feedback

Here, K_c is a linear optimal controller calculated by solving the algebraic Riccati equation. K_i is a relatively small integral gain chosen by trial and error ($K_i = 0.01$). As we discussed in the analysis, x_2 and x_3 are not suitable variables to control. Consequently, we chose to control a combination of x_1 and x_4 in the state feedback. Hence, the weight matrix for state errors in the Linear Quadratic Regulator design is on the form

$$Q_{lqr} = \text{diag}([q_1, 0, 0, q_4]). \quad (23)$$

4.4.2. Observability

Differential observability for high-gain observers is defined by Khalil [18] as follows. The system is differentially observable of order m if we can reconstruct x from the knowledge of y and u and their $m - 1$ first derivatives:

$$x(t) = \Phi(t, \bar{y}_{m-1}(t), \bar{u}_{m-1}(t)), \quad (24)$$

with the notation:

$$\bar{y}_{m-1}(t) = (y(t), \dots, y(t)^{(m-1)}) \quad (25)$$

This definition suggests that the states are observable if they are related to derivatives of the measurements and inputs. The structure of the model for the high-gain observer in [17, 18] is introduced as a chain of integrators where the measured state is at the end of the chain (e.g. measuring the position and estimating velocity in mechanical systems). The high-gain observer behaves like a differentiator, and the estimate is more accurate with a higher gain. This is similar to calculating the derivative by the finite difference by using a smaller step.

If we consider the structure of the four-state model with P_{rt} as the measurement, we indeed find a chain of integrators. The state x_3 , which is proportional to P_{rt}

in (A.17)-(A.18), is the integral of the gas flow rate at the riser base, $(w_G)_{\text{rb}}$. Also, $(w_G)_{\text{rb}}$ is related to P_{in} in (A.29) and (A.30). Thus, P_{rt} is related to the integral of P_{in} . In the other words, P_{in} is related to a derivative of P_{rt} . Therefore, the differential observability condition is satisfied when measuring the top pressure.

On the other hand, by measuring P_{in} , we have the opposite situation where we integrate the measured pressure to calculate P_{rt} and the associated state variables. For this case, the estimation is sensitive to modeling errors and disturbances. If an unknown model change or disturbance occurs, the observer continues to integrate the wrong conditions, and it will give different states \mathbf{x}' compared to the nominal states \mathbf{x} where there is no disturbance or error. Since the measured output and the input are the same $y(\mathbf{x}', u) = y(\mathbf{x}, u)$, the states are defined as *indistinguishable* [19]. Hence, the system is not observable from the measured output P_{in} .

4.4.3. High-gain Luenberger observer

When state variables for a state feedback controller are estimated by an observer, in addition to stabilizing properties of the controller and the observability of the system, another condition must be satisfied. That is the observer error dynamics converge to the origin exponentially fast [17, 18]. It is possible to satisfy this requirement by making the observer gain sufficiently large. Note that convergence rate of the observer must be considered, not only the magnitude of the observer gain. Such high-gain observers are robust to uncertainties in modeling the nonlinear functions.

The structure of the high-gain observer applied in this work is similar to the one used in [20]:

$$\begin{aligned} \dot{\hat{x}}_1 &= (w_G)_{\text{in}} - (w_G)_{\text{rb}} \\ \dot{\hat{x}}_2 &= (w_L)_{\text{in}} - (w_L)_{\text{rb}} \\ \dot{\hat{y}} &= f_3(\hat{x}) + \frac{1}{\epsilon}(y - \hat{y}) \\ \dot{\hat{x}}_4 &= (w_L)_{\text{rb}} - [1 - (\alpha_L^m)_{\text{rt}}]w_{\text{out}} \end{aligned} \quad (26)$$

where $\frac{1}{\epsilon}$ is the high gain. The observer states are \hat{x}_1 (mass of gas in pipeline), \hat{x}_2 (mass of liquid in pipeline), $\hat{y} = \hat{P}_{\text{rt}}$ (pressure at top of riser) and \hat{x}_4 (mass of liquid in riser). The measured output is $y = P_{\text{rt}}$ which is directly related to x_3 (ideal gas law),

$$P_{\text{rt}} = x_3 RT_{\text{r}} / [M_G (V_{\text{r}} - x_4 / \rho_L)]. \quad (27)$$

The third state equation $f_3(\hat{x})$ is obtained by the partial derivatives [21].

$$f_3(\hat{x}) = \dot{P}_{rt} = [\partial P_{rt}/\partial \hat{x}_3] \dot{\hat{x}}_3 + [\partial P_{rt}/\partial \hat{x}_4] \dot{\hat{x}}_4. \quad (28)$$

5. Experiments

5.1. Experimental setup

The experiments were carried out in laboratory setup for anti-slug control at the Chemical Engineering Department of NTNU. Figure 8 shows a schematic representation of the laboratory setup. The pipeline and the riser are made of flexible pipes with 2 cm inner diameters. The length of the pipeline is 4 m and it is inclined with a 15° angle. The height of the riser is 3 m. A buffer tank is used to simulate the effect of a long pipe with the same volume, such that the total length of pipe would be about 70 m.

The separator pressure after the topside choke valve is nominally constant at atmospheric pressure. The feed into the pipeline is assumed to be at constant flow rates, 4 liter/min of water and 4.5 liter/min of air. With these boundary conditions, the critical valve opening where the system switches from stable (non-slug) to oscillatory (slug) flow is at $Z^* = 15\%$.

5.2. Time delay and maximum valve opening

These experiments were performed on a set of descending pressure setpoints to observe where the system becomes unstable. The process is ‘open-loop stable’ for small valve opening and large pressure values which are indicated by the gray background on the figures. The objective is to operate outside and far from the shaded areas. In practice, a lower pressure setpoint gives a larger valve opening and a higher production rate. However, it is more difficult to stabilize the flow on low pressure setpoints.

To test the tolerance of the controllers to time delay, we repeated each experiment for three different values of time delay: 1 sec, 2 sec and 3 sec.

The feedback linearization controller stabilizes the system up to a 60% valve opening when no time delay is added (Figure 9). However, with a 2 sec time delay, it is stable only up to a 25% valve opening.

The feedback linearization design and proof of stability were done based on the riser base pressure P_{rb} . We tested the controller also with the inlet pressure P_{in} in experiments. A better performance is obtained by using P_{in} , because P_{in} is affected by noise less than P_{rb} .

The gain-scheduling IMC was able to stabilize the system up to a 60% valve opening (Figure 10), if no additional time delay is added. With a 2 sec time delay, it is stable up to a 50% valve opening.

The baseline controller for the adaptive PI was obtained from an IMC design with $\lambda = 24$ s which gives $K_c = 11.21$ and $\tau_I = 607.82$ s. Without adaptation, this controller gives a maximum valve opening was only 30%. Figure 11 shows the experimental result of the adaptive

Table 3: Maximum valve opening achieved by different controllers and different values of additional time delay

Controller	CV	additional time delay		
		$\theta = 0$	$\theta = 1$	$\theta = 2$
Gain-scheduling IMC	P_{in}	60%	60%	50%
Adaptive PI	P_{in}	60%	40%	32%
Feedback linearization	P_{in} & P_{rt}	60%	40%	25%
PI without adaptation	P_{in}	40%	40%	25%
Observer/ \mathcal{H}_∞ control	P_{rt}	38%	38%	35%
Observer/state feedback	P_{rt}	28%	24%	22%

PI controller. This controller was able to stabilize the system up to $Z = 60\%$ when no time delay was added, and $Z = 32\%$ with a 2 sec added time delay.

Then, We tested PI control with a fixed tuning ($K_c = 16.25$, $\tau_I = 213.69$ s). This tuning was obtained from IMC design with $\lambda = 15$ s. Figure 12 shows that the system is stable for all given setpoints. However, the controller could not bring the system to low pressure setpoints. Thus, there is an offset between the measurement and the setpoint, and the maximum valve opening is $Z = 40\%$.

Figure 13 shows the result of using the state feedback with the nonlinear observer scheme for control. It can stabilize the system up to a 28% valve opening. However, with a 2 sec time delay, it is stable only up to a 22% valve opening. Then, we replaced the state feedback by a robust \mathcal{H}_∞ controller where the controlled variable is the estimated inlet pressure. Substantially better results were achieved by the \mathcal{H}_∞ controller as shown in Figure 14.

Table 3 compares the maximum valve opening achieved by using the six controllers and applying different values of the time delay.

5.3. Disturbance rejection

Here, the controllers are tested experimentally for robustness against inflow disturbances. Figures 15, 16, 17, 18, and 19 show responses to inflow disturbances for different controllers.

The controller is off initially, and it is turned on after 5 minutes. The liquid flow rate is changed from its nominal value (4 liter/min) to 5.5 liter/min at 10 minutes that is a 30% step change. The air flow rate is changed from its nominal value (4.5 liter/min) to 6 liter/min at 20 minutes that is also a 30% step change.

The disturbance rejection tests for those controllers involving the high-gain observer are performed at $Z = 20\%$, because we do not expect them to work well at larger valve openings, while for the other controllers the tests are performed at $Z = 30\%$.

All of the controllers can handle the inflow disturbances and remain stable in the experiments. However, responses for observer-based controllers in Figures 18 and 19 show oscillations and larger offsets between actual pressure and the setpoint, compared to the other controllers.

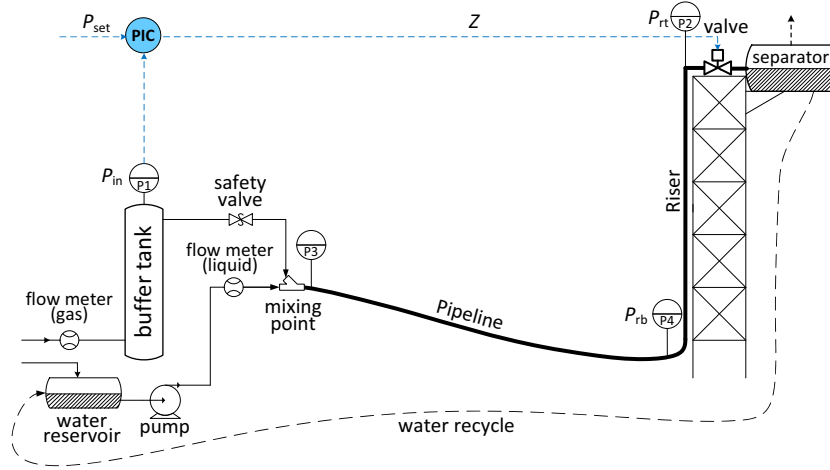


Figure 8: Schematic diagram of experimental setup

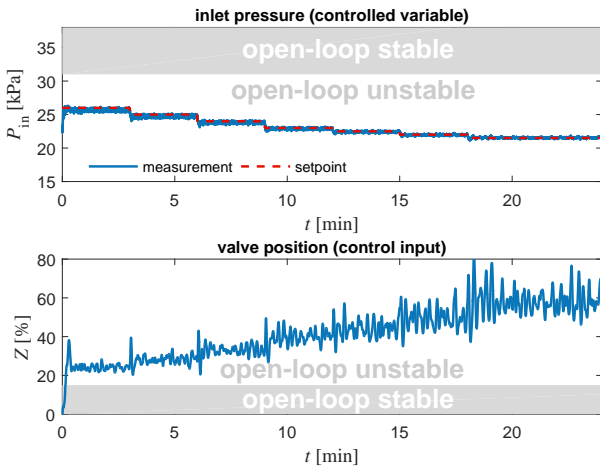


Figure 9: Feedback linearization controller, $CV = P_{in}$, $\theta = 0$ s

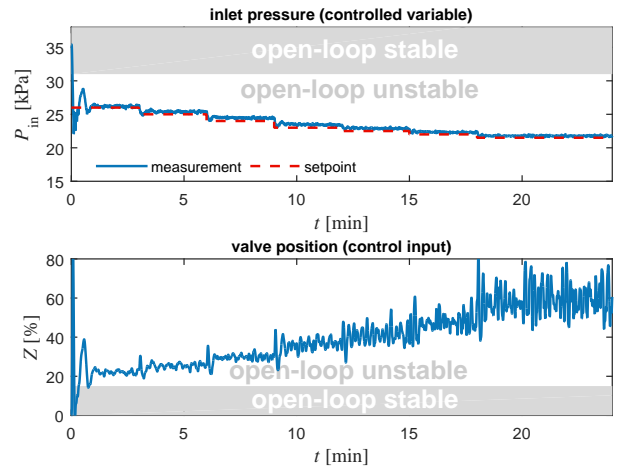


Figure 11: Adaptive PI controller, $CV = P_{in}$, $\theta = 0$ s

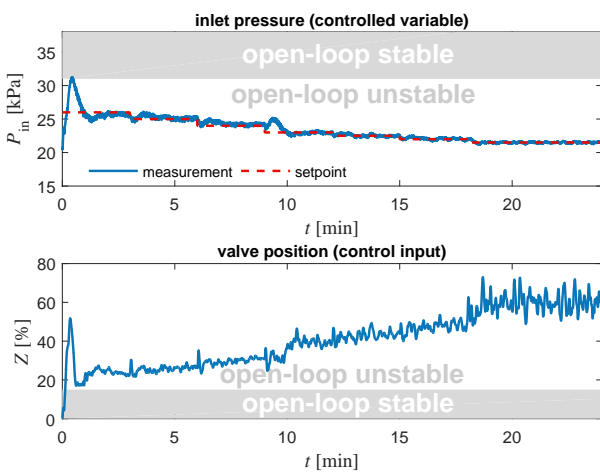


Figure 10: Gain-scheduling IMC, $CV = P_{in}$, $\theta = 0$ s

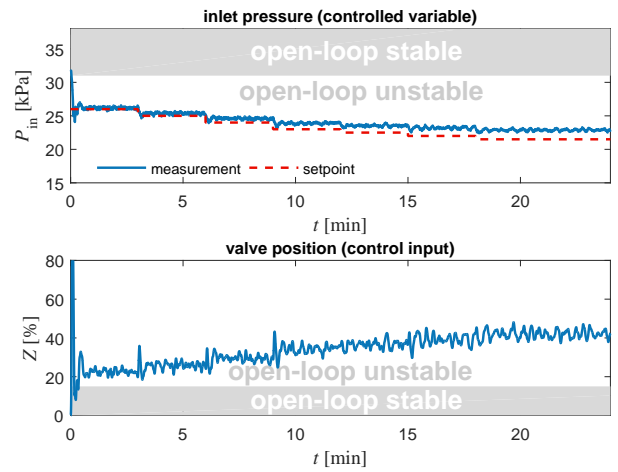


Figure 12: PI controller (without adaptation) tuned at $Z = 20\%$ with $K_c = -16.15$ and $\tau_I = 213.69$ s, $CV = P_{in}$, $\theta = 0$ s

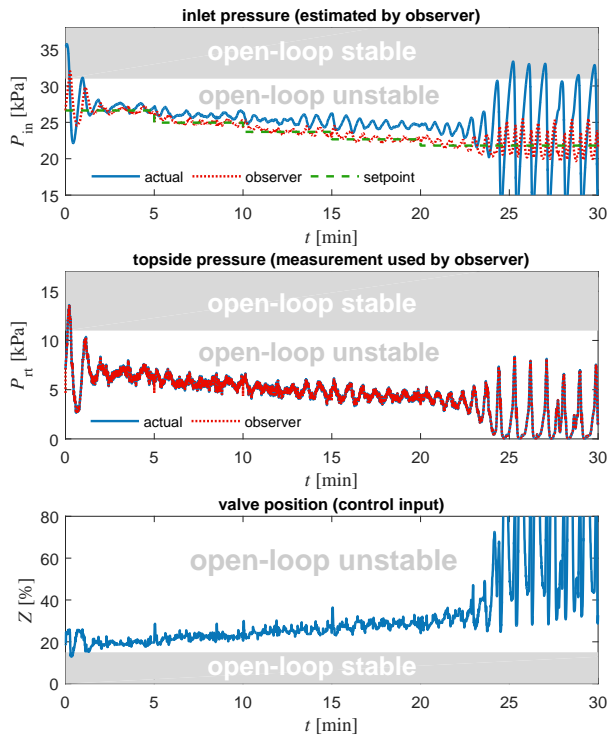


Figure 13: High-Gain observer/state feedback, $CV = P_{rt}$, $\theta = 0$ s

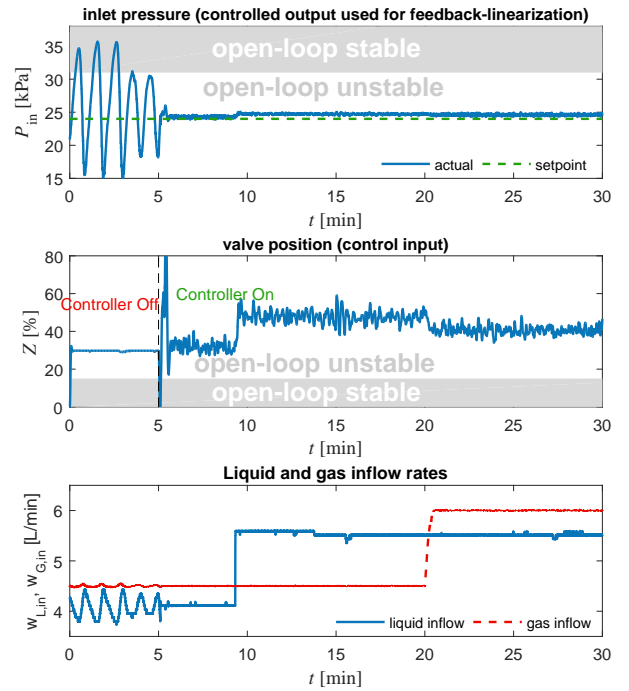


Figure 15: Response to inflow disturbances for feedback-linearization controller with $CV = P_{in}$ (control starts at 5 minutes)

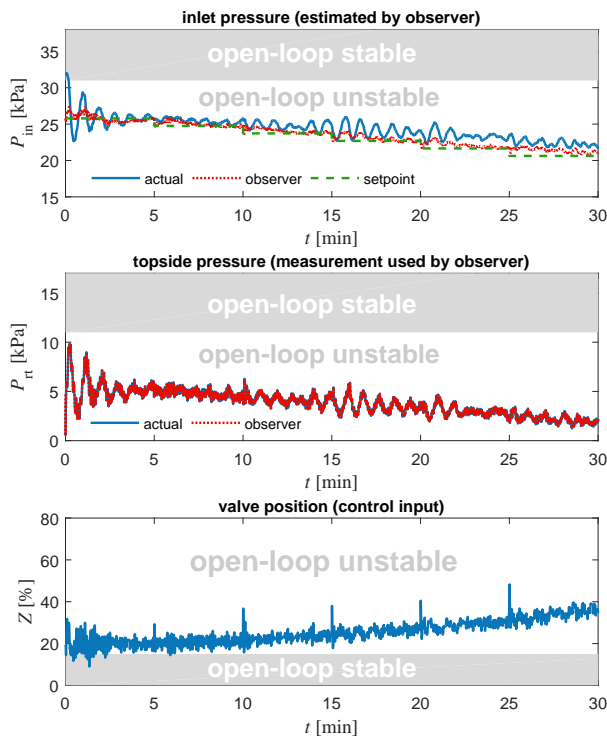


Figure 14: High-Gain observer/ \mathcal{H}_∞ controller, $CV = P_{rt}$, $\theta = 0$ s

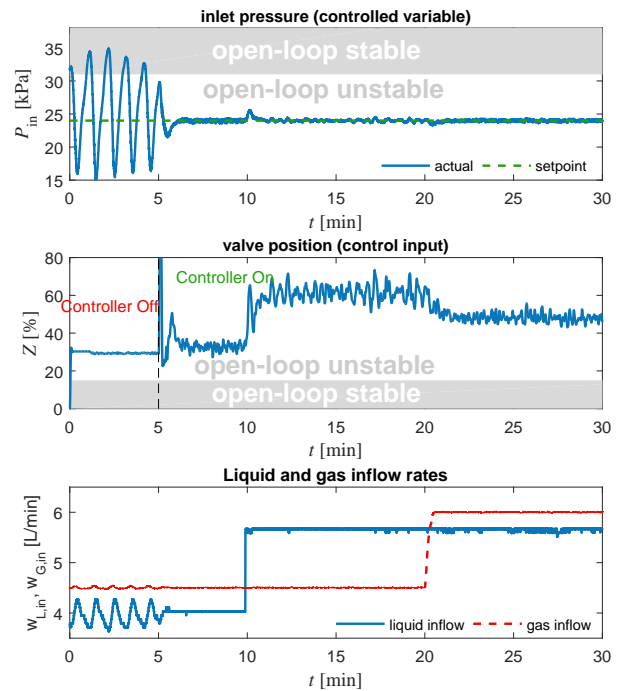


Figure 16: Response to inflow disturbances for gain scheduling controller with $CV = P_{in}$ (control starts at 5 minutes)

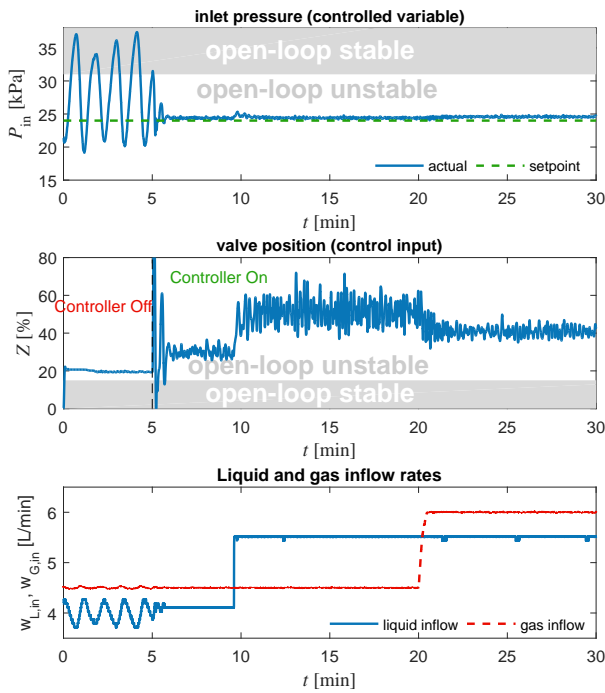


Figure 17: Response to inflow disturbances for adaptive PI controller with $CV = P_{in}$ (control starts at 5 minutes)

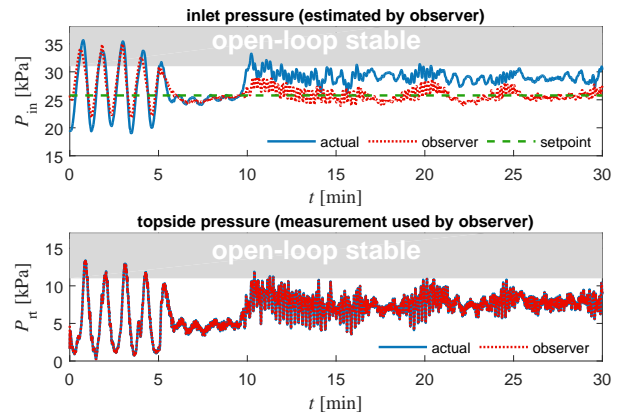


Figure 19: Response to inflow disturbances for High-Gain observer/ \mathcal{H}_∞ controller with $CV = P_{rt}$ (control starts at 5 minutes)

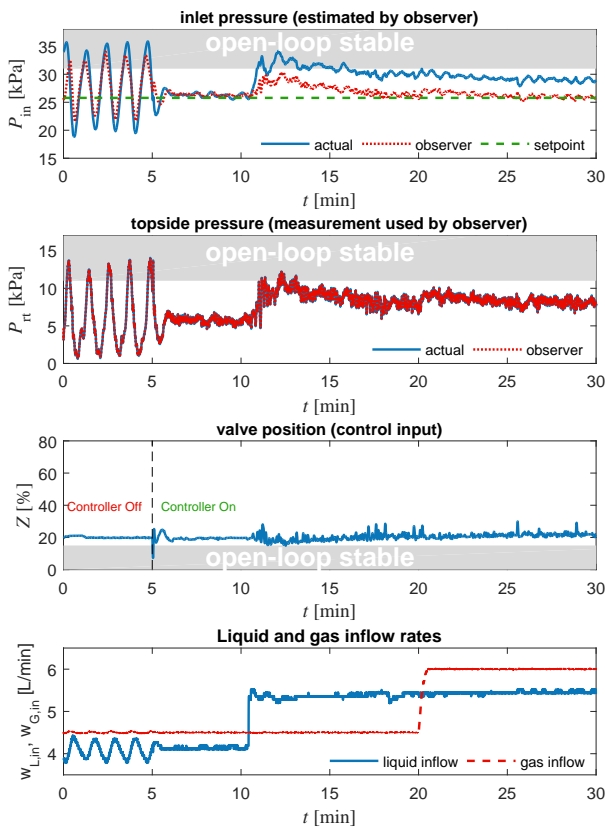


Figure 18: Response to inflow disturbances for High-Gain observer/state feedback with $CV = P_{rt}$ (control starts at 5 minutes)

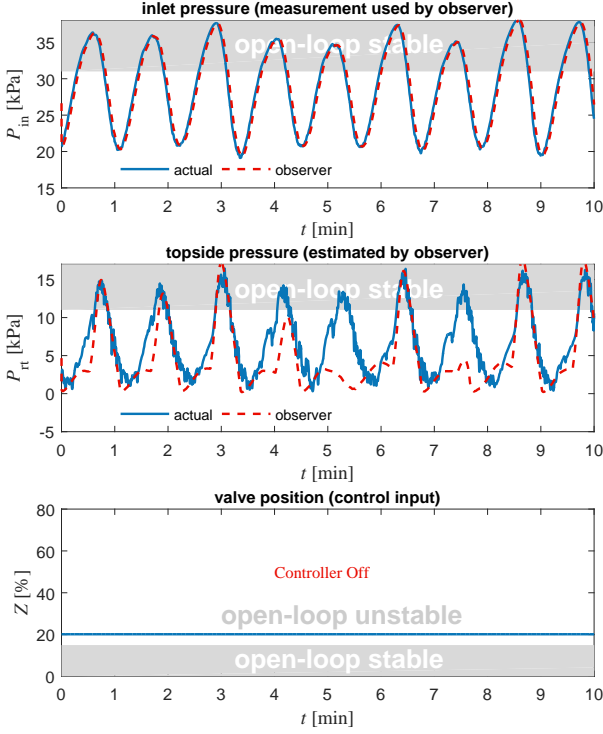


Figure 20: High-gain observer in open-loop, $y_m = P_{in}$, $Z = 20\%$

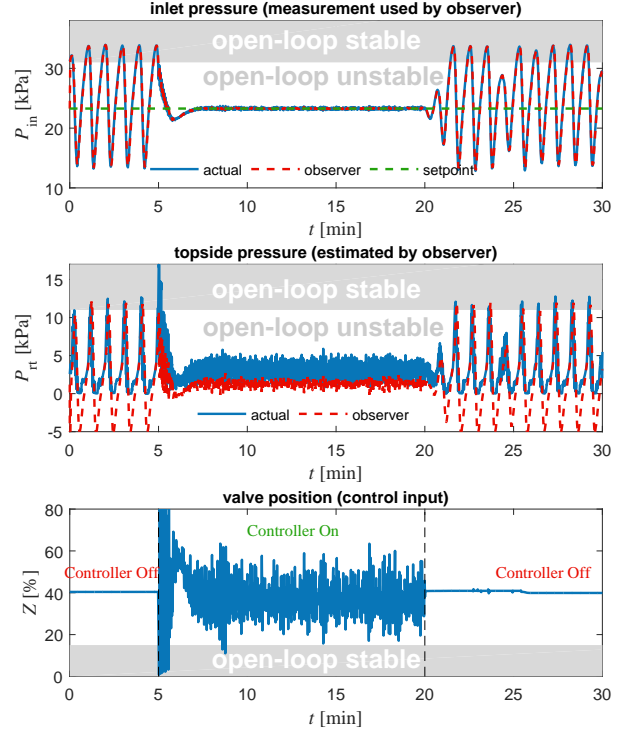


Figure 21: Linear KF/state feedback, $CV = P_{in}$, $Z = 40\%$

5.4. Observability test

As expected from the observability conditions, it was not possible to stabilize the process when we used the high-gain observer measuring the inlet pressure P_{in} . The observer diverges, and P_{rt} with its related state variables is not correctly estimated. Consequently, the state feedback cannot stabilize the process. This happens when we increase the gain of the observer for the supposed robustness of the closed-loop system. Figure 20 shows the result of the open-loop estimation using a Luenberger observer with a large gain ($\epsilon = 10^{-4}$), where P_{in} is the measurement used by the observer.

On the other hand, we used a linear Kalman filter with the P_{in} measurement, and it was possible to stabilize the system up to a $Z = 40\%$ valve opening (Figure 21).

We also tested ‘slow’ Luenberger observers ($\epsilon = 1$) experimentally. It was possible to produce estimates of the states by measuring either P_{in} or P_{rt} . Nevertheless, the closed-loop system was not robust and became unstable in most of the experimental runs. This observation is in agreement with the theory that the time-scale separation between the observer and the controller is necessary. That is the observer error dynamics must be faster than the stabilizing controller dynamics [17]. We summarize the performance of different observers for the state estimation in Table 4, and for the state feedback control in Table 5.

5.5. Observer convergence rate

Real states are not available to investigate the convergence rate of the observer; the subsea pressure is used for

this purpose. In Figure 22, we show the initial transient response of the observer. The topside pressure which is the measurement used by the observer converges immediately, but it takes around 60 s for the subsea pressure to converge. The convergence speed also depends on the system dynamics that act as a filter for this case. Generally, the high-gain observers suffer from noise effect, but the estimates are not affected by the noise for this case because of the filtering effect of the model.

6. Discussion

6.1. Combined nonlinearity and inverse response

It was not possible to stabilize the flow by controlling P_{rt} applying a linear controller directly. Different PI tunings have been tried in experiments and OLGA simulations. However, the process is stabilized when P_{rt} is used to estimate the states by a fast nonlinear observer, and applying a linear state feedback.

Table 4: State estimation using different observers

Observer	measured variable	
	P_{in}	P_{rt}
Fast linear observer	converges	diverges
Fast nonlinear observer	diverges	converges
Slow nonlinear observer	converges	converges

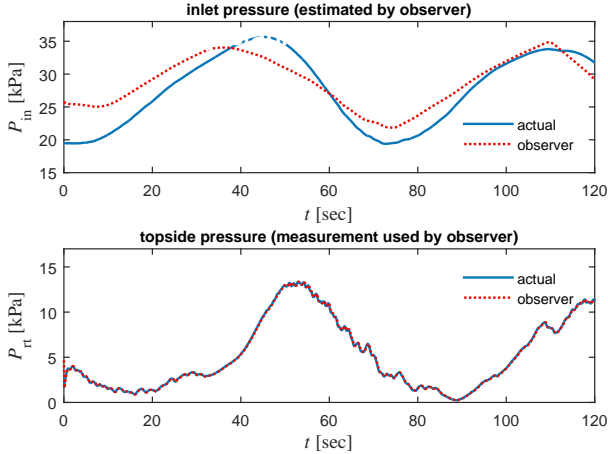


Figure 22: Visual evaluation of observer convergence rate by zooming on the initial transient response

In numerical simulations for the system analysis, it was possible to stabilize by controlling the P_{rt} using a robust \mathcal{H}_∞ controller only around the operating point where the process remains linear ($\Delta P = 0.1$ kPa); it was unstable for a larger setpoint change ($\Delta P = 1$ kPa). This confirms that the nonlinearity is an effective factor.

In addition to the nonlinearity, modeling errors and the measurement noise exist in experiments. Linear controllers require a good gain margin to be robust against both the nonlinearity and modeling errors. However, the necessary gain margin for the linear controllers is not achievable for P_{rt} because of RHP-zero dynamics. While both the nonlinearity and the inverse response are problematic for the control of the topside pressure in experiments, the nonlinear observer counteracts some of the nonlinearities and helps for robustness.

6.2. Observability

The linear Kalman Filter works well measuring the subsea pressure, but the nonlinear high-gain diverges when using this measurement. The Kalman observability for linear systems (rank condition) and the differential observability do not give the same results for this case. Note the (linear) Kalman observability is a necessary condition, but it is not sufficient.

In the case of the linear observer, we assume the correct stationary point, and we only deal with the deviations.

Table 5: Closed-loop performance where observers are used as state estimator for state feedback.

State estimator	measured variable	
	P_{in}	P_{rt}
Fast linear observer	robust	unstable
Fast nonlinear observer	unstable	stable
Slow nonlinear observer	not robust	not robust

Consequently, as shown in Figure 21, the estimation of the linear observer is less accurate, but it does not fail to stabilize the system.

6.3. Other remarks

The inflow rate in real systems is pressure-driven. For the analysis, we have made the inflow rates pressure-driven which is closer to the reality. However, the experimental setup used in this work is not able to simulate the pressure-driven inflow rates same as in the real systems. Hence, we have assumed constant inflow rates for the control designs and experiments. This issue might have implications on the final results of experiments.

Large offsets were observed between the measured subsea pressure and the setpoint for the controllers involving the high-gain observer. The reason is that the observer has been designed based on the four-state model with constant inflow rates. The inflow disturbances are assumed to be unknown to the control system, and they are not seen by the observer. This issue may be resolved by augmenting the inflow rates to the state vector which requires a different observer design.

The gain-scheduling IMC controller has a better tolerance to the time delay than the other controllers. The reason is the derivative action of the IMC controller which provides a larger phase margin.

Although the feedback linearization controller does not include integral action, it can track the setpoints and reject the disturbances in the experiments. The bias of the control signal is calculated by the nonlinear functions of the controller, and its accuracy is dependent on the model. Another drawback of this controller is that tuning of the linear part of the controller K_1 is done by trial and error which may not give the best result.

7. Conclusion

The system nonlinearity is a major reason for robustness issues in anti-slug control, and linear controllers require a good gain margin for the robustness. The static nonlinearity of the process follows the valve equation. An adaptive PI controller based on the static gain of the process was successfully applied to counteract the nonlinearity.

A gain-scheduling of linear controllers is well-suited for anti-slug control when a subsea pressure measurement is available. Compared to the nonlinear controllers based on the mechanistic model, the gain-scheduling controller is more robust and requires less modeling effort. To use the mechanistic model for control, many parameters and physical values of the process are needed to configure the model.

If the subsea pressure is not available, we can recover considerable stabilizability by using a nonlinear high-gain observer and controlling the estimates. The high-gain observer was tested successfully in combinations with a state

595 feedback controller and a robust \mathcal{H}_∞ controller. This so-
 lution was applicable for smaller valve openings than what
 achieved by control of the subsea pressure. Nevertheless,⁶⁶⁰
 the benefit regarding the production rate may not be sig-
 nificant by controlling at very large valve openings.

600 The Kalman observability rank condition is satisfied
 for the subsea pressure output, and a linear Kalman filter⁶⁶⁵
 was tested successfully in experiments. However, the non-
 linear high-gain observer diverges, because the states are
indistinguishable and the system is not observable from a
 605 differential observability point of view.⁶⁷⁰

Acknowledgements

Financial support for this research was provided by
 SIEMENS AS, Norway.

References

- 610 [1] Y. Taitel, Stability of severe slugging, *International Journal of
 Multiphase Flow* 12 (2) (1986) 203–217.
- [2] A. Courbot, Prevention of severe slugging in the dunbar 16
 inches multiphase pipeline, in: *Proceedings of the Annual
 Offshore Technology Conference*, Vol. 4, 1996, pp. 445–452,
 615 *SPE no.* 8196.
- [3] K. Havre, K. Stornes, H. Stray, Taming slug flow in pipelines,
ABB Review 4 (2000) 55–63.
- [4] J.-M. Godhavn, M. P. Fard, P. H. Fuchs, New slug control
 strategies, tuning rules and experimental results, *Journal of Pro-
 cess Control* 15 (2005) 547–557.
- 620 [5] E. Jahanshahi, S. Skogestad, Simplified dynamic models for
 control of riser slugging in offshore oil production, *SPE Oil and
 Gas Facilities* 3 (6) (2014) 64–79.
- [6] J.-M. Godhavn, Email communication, private communication
 625 (2016).
- [7] E. Storakaas, S. Skogestad, Controllability analysis of two-phase
 pipeline-riser systems at riser slugging conditions, *Control En-
 gineering Practice* 15 (5) (2007) 567–581.
- [8] O. Aamo, G. Eikrem, H. Siahaan, B. Foss, Observer design
 for multiphase flow in vertical pipes with gas-lift - theory and
 630 experiments, *Journal of Process Control* 15 (3) (2005) 247 –
 257.
- [9] F. D. Meglio, N. Petit, V. Alstad, G.-O. Kaasa, Stabilization
 of slugging in oil production facilities with or without upstream
 pressure sensors, *Journal of Process Control* 22 (4) (2012) 809
 – 822. doi:10.1016/j.jprocont.2012.02.014.
- 635 [10] E. Jahanshahi, S. Skogestad, Comparison between nonlinear
 model-based controllers and gain-scheduling internal model con-
 trol based on identified model, in: *Decision and Control (CDC),
 2013 IEEE 52nd Annual Conference on*, 2013, pp. 853–860.
 doi:10.1109/CDC.2013.6759989.
- [11] K. H. Bendiksen, D. Malnes, R. Moe, S. Nuland, Dynamic two-
 fluid model olga. theory and application, *SPE Production En-
 gineering* 6 (2) (1991) 171–180.
- 640 [12] T. Schweickhardt, F. Allgower, F. Doyle, Nonlinearity quanti-
 fication for the optimal state feedback controller, in: *European
 Control Conference (ECC)*, 2003, pp. 330–335.
- [13] S. Skogestad, I. Postlethwaite, *Multivariable Feedback Control:
 Analysis and Design*, Wiley & Sons, Chichester, West Sussex,
 645 UK, 2005.
- [14] E. Jahanshahi, Advanced control solutions for multiphase flow:
 Linear and nonlinear approaches to anti-slug control, Phd thesis,
 Norwegian University of Science and Technology (2013).
- [15] E. Jahanshahi, S. Skogestad, Anti-slug control solutions based
 650 on identified model, *Journal of Process Control* 30 (2015) 58 –
 68. doi:10.1016/j.jprocont.2014.12.007.

- [16] M. Morari, E. Zafriou, *Robust Process Control*, Prentice Hall,
 Englewood Cliffs, New Jersey, 1989.
- [17] H. K. Khalil, *Nonlinear Systems*, Third Edition, Prentice Hall,
 Upper Saddle River, New Jersey, 2002.
- [18] H. K. Khalil, L. Praly, High-gain observers in nonlinear feedback
 control, *International Journal of Robust and Nonlinear Control*
 24 (6) (2014) 991–992. doi:10.1002/rnc.3156.
- [19] R. Hermann, A. Krener, Nonlinear controllability and observ-
 ability, *IEEE Transactions on Automatic Control* 22 (5) (1977)
 728–740. doi:10.1109/TAC.1977.1101601.
- [20] F. Di Meglio, G.-O. Kaasa, N. Petit, V. Alstad, Reproducing
 slugging oscillations of a real oil well, in: *49th IEEE Confer-
 ence on Decision and Control*, Atlanta, Georgia, USA, 2010,
 pp. 4473–4479.
- [21] E. Jahanshahi, S. Skogestad, E. I. Grøtli, Anti-slug control ex-
 periments using nonlinear observer, in: *American Control Con-
 ference*, Washington D.C., 2013, pp. 1056–1062.

A. Appendix: Model equations

A.1. Pipeline model

$$\langle \rho_G \rangle_P = P_{\text{in,nom}} M_G / (RT_P) \quad (\text{A.1})$$

$$\langle \alpha_L \rangle_P = \frac{\langle \rho_G \rangle_P (w_L)_{\text{in}}}{\langle \rho_G \rangle_P (w_L)_{\text{in}} + \rho_L (w_G)_{\text{in}}} \quad (\text{A.2})$$

$$\langle h \rangle = K_h \langle \alpha_L \rangle_P D_P / \cos(\theta) \quad (\text{A.3})$$

$$\langle x_2 \rangle = \rho_L V_P \langle \alpha_L \rangle_P \quad (\text{A.4})$$

$$h = \langle h \rangle + \left(\frac{x_2 - \langle x_2 \rangle}{A_P (1 - \langle \alpha_L \rangle_P) \rho_L} \right) \sin(\theta) \quad (\text{A.5})$$

$$\langle \rho_G \rangle_P = \frac{x_1}{V_P - x_2 / \rho_L} \quad (\text{A.6})$$

$$P_{\text{in}} = \langle \rho_G \rangle_P RT_P / M_G \quad (\text{A.7})$$

$$\langle U_{\text{SG}} \rangle_P = \frac{(w_G)_{\text{in}}}{\langle \rho_G \rangle_P A_P} \quad (\text{A.8})$$

$$\langle U_{\text{SL}} \rangle_P = \frac{(w_L)_{\text{in}}}{\rho_L A_P} \quad (\text{A.9})$$

$$\langle U_{\text{m}} \rangle_P = \langle U_{\text{SL}} \rangle_P + \langle U_{\text{SG}} \rangle_P \quad (\text{A.10})$$

$$\langle \rho_{\text{m}} \rangle_P = \langle \alpha_L \rangle_P \rho_L + [1 - \langle \alpha_L \rangle_P] \langle \rho_G \rangle_P \quad (\text{A.11})$$

$$\langle \mu_{\text{m}} \rangle_P = \langle \alpha_L \rangle_P \mu_L + [1 - \langle \alpha_L \rangle_P] \mu_G \quad (\text{A.12})$$

$$\langle N_{\text{Re}} \rangle_P = \frac{\langle \rho_{\text{m}} \rangle_P \langle U_{\text{m}} \rangle_P D_P}{\langle \mu_{\text{m}} \rangle_P} \quad (\text{A.13})$$

$$\lambda_P = 0.0056 + 0.5 \langle N_{\text{Re}} \rangle_P^{-0.32} \quad (\text{A.14})$$

$$\langle \Delta P_f \rangle_P = \frac{\lambda_P \rho_L \langle u_{\text{SL}} \rangle_P^2 L_P}{2 D_P} \quad (\text{A.15})$$

A.2. Riser model

$$\langle V_G \rangle_r = A_r (L_r + L_h) - x_4 / \rho_L \quad (\text{A.16})$$

$$\langle \rho_G \rangle_r = x_3 / \langle V_G \rangle_r \quad (\text{A.17})$$

$$P_{\text{rt}} = \frac{\langle \rho_G \rangle_r RT_r}{M_G} \quad (\text{A.18})$$

$$\langle \alpha_L \rangle_r = \frac{x_4}{A_r(L_r + L_h)\rho_L} \quad (\text{A.19})^{675}$$

$$\langle \rho_m \rangle_r = \frac{x_3 + x_4}{A_r(L_r + L_h)} \quad (\text{A.20})$$

$$\langle U_{sL} \rangle_r = \frac{(w_L)_{in}}{\rho_L A_r} \quad (\text{A.21})$$

$$\langle U_{sG} \rangle_r = \frac{(w_G)_{in}}{(\rho_G)_r A_r} \quad (\text{A.22})$$

$$\langle U_m \rangle_r = \langle U_{sL} \rangle_r + \langle U_{sG} \rangle_r \quad (\text{A.23})$$

$$\langle \mu_m \rangle_r = \langle \alpha_L \rangle_r \mu_L + [1 - \langle \alpha_L \rangle_r] \mu_G \quad (\text{A.24})$$

$$(N_{Re})_r = \frac{\langle \rho_m \rangle_r \langle U_m \rangle_r D_r}{\langle \mu_m \rangle_r} \quad (\text{A.25})$$

$$\frac{1}{\sqrt{\lambda_r}} = -1.8 \log_{10} \left[\left(\frac{\epsilon/D_r}{3.7} \right)^{1.11} + \frac{6.9}{(N_{Re})_r} \right] \quad (\text{A.26})$$

$$(\Delta P_f)_r = \frac{\lambda_r \langle \rho_m \rangle_r \langle U_m \rangle_r^2 (L_r + L_h)}{2D_r}, \quad (\text{A.27})$$

A.3. Gas flow model at riser base

$$A_G = \begin{cases} A_p \left(\frac{D_p - h \cos \theta}{D_p} \right)^2, & \text{if } h \cos \theta < D_p \\ 0, & \text{if } h \cos \theta \geq D_p \end{cases} \quad (\text{A.28})$$

$$\Delta P_G = P_{in} - (\Delta P_f)_p - P_{rt} - \langle \rho_m \rangle_r g L_r - (\Delta P_f)_r \quad (\text{A.29})$$

$$(w_G)_{rb} = \begin{cases} K_G A_G \sqrt{(\rho_G)_p \Delta P_G}, & \text{if } h \cos \theta < D_p \\ 0, & \text{if } h \cos \theta \geq D_p \end{cases} \quad (\text{A.30})$$

A.4. Liquid flow model at riser base

$$(\alpha_L)_{rb} = (A_p - A_G)/A_p \quad (\text{A.31})$$

$$\Delta P_L = P_{in} - (\Delta P_f)_p + \rho_L g h - P_{rt} - \langle \rho_m \rangle_r g L_r - (\Delta P_f)_r \quad (\text{A.32})$$

$$(w_L)_{rb} = K_L (A_p - A_G) \sqrt{\rho_L \Delta P_L} \quad (\text{A.33})$$

A.5. Outlet boundary conditions

$$(\alpha_L)_{rt} = \begin{cases} \langle \alpha_L \rangle_r, & \text{if } (\alpha_L)_{rb} \leq \langle \alpha_L \rangle_r; \\ 2\langle \alpha_L \rangle_r - (\alpha_L)_{rb}, & \text{if } \langle \alpha_L \rangle_r < (\alpha_L)_{rb} < 2\langle \alpha_L \rangle_r; \\ 0, & \text{if } (\alpha_L)_{rb} \geq 2\langle \alpha_L \rangle_r \end{cases} \quad (\text{A.34})$$

$$\rho_{rt} = (\alpha_L)_{rt} \rho_L + [1 - (\alpha_L)_{rt}] (\rho_G)_r \quad (\text{A.35})$$

$$(\alpha_L^m)_{rt} = \frac{(\alpha_L)_{rt} \rho_L}{(\alpha_L)_{rt} \rho_L + [1 - (\alpha_L)_{rt}] (\rho_G)_r} \quad (\text{A.36})$$

$$w_{out} = C_v f(z) \sqrt{\rho_{rt} \max(P_{rt} - P_s, 0)} \quad (\text{A.37})$$

$$(w_L)_{out} = (\alpha_L^m)_{rt} w_{out} \quad (\text{A.38})$$

$$(w_G)_{out} = [1 - (\alpha_L^m)_{rt}] w_{out} \quad (\text{A.39})$$

Table A.6: Model parameters and variables

Symbol	Description	Unit
Constants		
R	Universal gas constant	J/(kmol.K)
g	Gravity	m/s ²
μ_L	Liquid viscosity	Pa.s
μ_G	Gas viscosity	Pa.s
ϵ	Pipe roughness	m
ρ_L	Liquid density	kg/m ³
M_G	Gas molecular weight	gr
T_p	Fluid temperature in pipeline	°K
V_p	Pipe volume	m ³
D_p	Pipe diameter	m
A_p	Pipe cross section area	m ²
L_p	Pipe length	m
T_r	Fluid temperature in riser	°K
V_r	Riser volume	m ³
D_r	Riser diameter	m
A_r	Riser cross section area	m ²
L_r	Riser length	m
L_h	Length of horizontal section	m
P_s	Separator pressure	bar
$(w_L)_{in}$	Inlet liquid mass flow	kg/s
$(w_G)_{in}$	Inlet gas mass flow	kg/s
K_h	Coefficient for level of liquid in pipe	–
K_G	Coefficient for riser base gas flow	–
K_L	Coefficient for riser base liquid flow	–
C_v	Production choke valve constant	m ²
Variables		
x_1	Mass of gas in pipeline	kg
x_2	Mass of liquid in pipeline	kg
x_3	Mass of gas in riser	kg
x_4	Mass of liquid in riser	kg
$(w_G)_{rb}$	Mass flow rate of gas at riser base	kg/s
$(w_L)_{rb}$	Mass flow rate of liquid at riser base	kg/s
$(w_G)_{out}$	Mass flow rate of outlet gas	kg/s
$(w_L)_{out}$	Mass flow rate of outlet liquid	kg/s
w_{out}	Mass flow rate of outlet mixture	kg/s
ρ_{rt}	Mixture density at top of riser	kg/m ³
P_{rt}	Pressure at top of riser	Pa
$(\alpha_L^m)_{rt}$	Liquid mass fraction at top of riser	kg/kg
$(\alpha_L)_{rt}$	Liquid volume fraction at top of riser	m ³ /m ³
$(\rho_G)_r$	Gas density in riser	kg/m ³
$\langle \alpha_L^m \rangle_p$	Average liquid mass fraction in pipe	kg/kg
$\langle \alpha_L \rangle_p$	Average liquid volume fraction in pipe	m ³ /m ³
$\langle \rho_G \rangle_p$	Average gas density in pipe	kg/m ³
$P_{in,nom}$	Steady-state pressure at pipe inlet	Pa
$\langle x_2 \rangle$	Average mass of liquid in pipe	kg
$\langle h \rangle$	Average level of liquid at low-point	m
h	Level of liquid in pipe	m
$(V_G)_p$	Volume of gas in pipe	m ³
P_{in}	Pressure at inlet of pipe	Pa
$(\Delta P_f)_p$	Friction pressure loss in pipe	Pa
λ_p	Friction factor in pipe	–
$(N_{Re})_p$	Reynolds number of flow in pipe	–
$\langle \rho_m \rangle_p$	Average mixture density in pipe	kg/m ³
$\langle \mu_m \rangle_p$	Average mixture viscosity in pipe	Pa.s
$\langle U_m \rangle_p$	Average mixture velocity in pipe	m/s
$\langle U_{sG} \rangle_p$	Average superficial vel. of gas in pipe	m/s

Continued on next column

Continued from previous column

Symbol	Description	Unit
$\langle U_{sL} \rangle_p$	Average superficial vel. of liq. in pipe	m/s
$\langle V_G \rangle_r$	Volume of gas in riser	m ³
$\langle \alpha_L \rangle_r$	Average liquid volume fraction in riser	m ³ /m ³
$\langle \rho_m \rangle_r$	Average mixture density inside riser	kg/m ³
$\langle \Delta P_f \rangle_r$	Friction pressure loss of riser	Pa
λ_r	Friction factor in riser	–
$\langle N_{Re} \rangle_r$	Reynolds number of flow in riser	–
$\langle U_m \rangle_r$	Average mixture velocity in riser	m/s
$\langle U_{sL} \rangle_r$	Average superficial vel. of liquid in riser	m/s
$\langle U_{sG} \rangle_r$	Average superficial vel. of gas in riser	m/s
$\langle \mu_m \rangle_r$	Average mixture viscosity in riser	Pa.s
ΔP_G	Diff. pressure for riser base gas flow	Pa
A_G	Free area for gas flow at low-point	m ²
ΔP_L	Diff. pressure for riser base liquid flow	Pa
A_L	Area for liquid flow at riser base	m ²
$\langle \alpha_L \rangle_{rb}$	Liquid volume fraction at riser base	m ³ /m ³

B. Appendix: Static Gain Model

From the valve equation in (7), we get

$$\Delta P_v = \left(\frac{w_{out}^2}{C_v^2} \right) \frac{1}{f(Z)^2 \rho_{rt}}. \quad (B.1)$$

The riser top pressure is

$$P_{rt} = P_s + (\Delta P)_v, \quad (B.2)$$

and the steady-state inlet pressure is expressed as follows.

$$(P_{in})_{ss} = P_s + (\Delta P_v)_{ss} + \rho_{ss} g L_r + \Delta P_f, \quad (B.3)$$

where the subscript 'ss' denotes the steady-state. The mixture density ρ_{rt} in (B.1) can be replaced by the steady-state density ρ_{ss} obtained by combining (A.2) and (A.35).

$$\rho_{ss} = \frac{w_{out} \rho_L \rho_G}{(w_G)_{in} \rho_L + (w_L)_{in} \rho_G} \quad (B.4)$$

The specific volume is on the form

$$\nu_{ss} = \frac{1}{\rho_{ss}} = \frac{(w_L)_{in}}{w_{out} \rho_G} + \frac{(w_G)_{in}}{w_{out} \rho_L}. \quad (B.5)$$

Note that $w_{out} = (w_G)_{in} + (w_L)_{in}$ for the steady-state.

In (B.4) and (B.5), the liquid density ρ_L is constant and the gas density ρ_G depends on the top pressure by ideal gas law in (A.18). With $\Delta P_v = P_{rt} - P_s$, we get

$$\rho_G = c_1 \Delta P_v + c_0, \quad (B.6)$$

where $c_1 = M_G/(RT_r)$ and $c_0 = c_1 P_s$ are constants. We define $u = C_v f(z)$, and calculate the partial derivatives:

$$\frac{\partial \rho_{ss}}{\partial \Delta P_v} = \frac{c_1 \rho_{ss}^2 (w_G)_{in}}{\rho_G^2 w_{out}} \quad (B.7)$$

$$\frac{\partial \nu_{ss}}{\partial \Delta P_v} = \frac{-c_1 (w_G)_{in}}{\rho_G^2 w_{out}} \quad (B.8)$$

$$\frac{\partial (\Delta P_v)_{ss}}{\partial u} = \left(\frac{\partial \nu_{ss}}{\partial (\Delta P_v)_{ss}} \frac{\partial \Delta P_v}{\partial u} \right) \frac{w_{out}^2}{u^2} + \frac{-2\nu_{ss} w_{out}^2}{u^3} \quad (B.9)$$

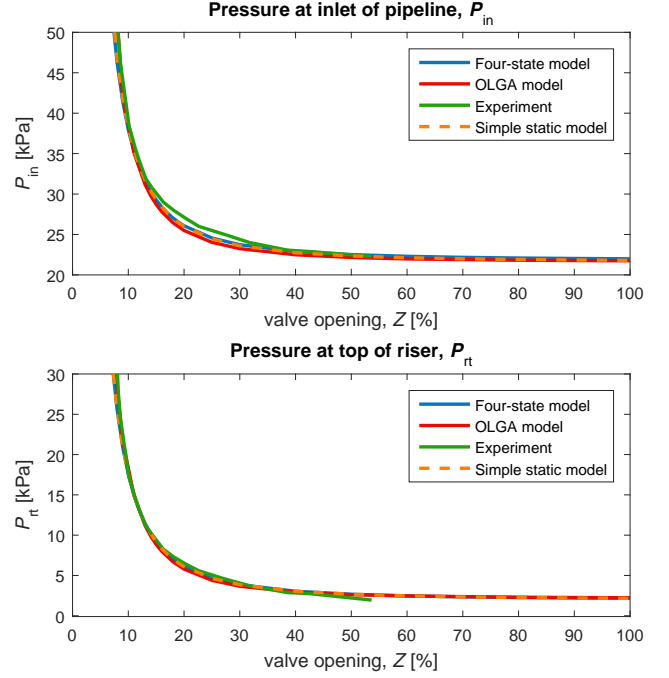


Figure B.23: Simple static model (dashed line) compared to other models (solid lines)

$$\frac{\partial (\Delta P_v)_{ss}}{\partial u} = \frac{-2 (\Delta P_v)_{ss}}{u \left(1 + \frac{c_1 (w_G)_{in} w_{out}}{u^2 \rho_G^2} \right)} \quad (B.10)$$

$$\frac{\partial (P_{in})_{ss}}{\partial u} = \frac{\partial (\Delta P_v)_{ss}}{\partial u} + gL \left(\frac{\partial \rho_{ss}}{\partial \Delta P_v} \frac{\partial (\Delta P_v)_{ss}}{\partial u} \right) \quad (B.11)$$

By combining (B.7) and (B.11), we get

$$\frac{\partial (P_{in})_{ss}}{\partial u} = \frac{\partial (\Delta P_v)_{ss}}{\partial u} \left(1 + \frac{gL c_1 \rho_{ss}^2 (w_G)_{in}}{\rho_G^2 w_{out}} \right). \quad (B.12)$$

By applying (B.10), we have

$$\frac{\partial (P_{in})_{ss}}{\partial u} = \frac{\left(1 + \frac{gL c_1 \rho_{ss}^2 (w_G)_{in}}{\rho_G^2 w_{out}} \right) - 2 (\Delta P_v)_{ss}}{\left(1 + \frac{c_1 (w_G)_{in} w_{out}}{u^2 \rho_G^2} \right) u}, \quad (B.13)$$

$$\frac{\partial (P_{in})_{ss}}{\partial Z} = \left(\frac{\rho_G^2 + c_1 \Delta P_r \alpha_G^m}{\rho_G^2 + c_1 \Delta P_v \alpha_G^m} \right) \frac{-2 (\Delta P_v)_{ss}}{f(Z)} \frac{\partial f(Z)}{\partial Z}, \quad (B.14)$$

where $\Delta P_r = \rho_{ss} g L_r$ is the riser hydrostatic pressure drop, and α_G^m is the gas mass fraction:

$$\alpha_G^m = \frac{(w_G)_{in}}{(w_G)_{in} + (w_L)_{in}} \quad (B.15)$$

The gas mass fraction α_G^m is dependant on the GOR. Figure B.23 compares the steady-state pressure models in (B.2) and (B.3) with the full four-state model, the OLGA model and experiments. Here, we have applied $\alpha_G^m = 0.0015$, $c_1 = 0.0121 \text{ kg}/(\text{kPa} \cdot \text{m}^3)$ and $c_0 = 1.2514 \text{ kg}/\text{m}^3$. The constant friction term ΔP_f in (B.3) was treated as a tuning parameter, $\Delta P_f = 6 \text{ kPa}$.